

Monte Carlo, blocking, and inference: How to measure the renormalization group flow

Luca Di Carlo

*Joseph Henry Laboratories Department of Physics,
Princeton University, Princeton, New Jersey 08544, USA*

(Dated: January 11, 2024)

Abstract

Renormalization group theory is a powerful and intriguing technique with a wide range of applications. One of the main successes of renormalization group theory is the description of continuous phase transitions and the development of scaling theory. Most courses on phase transitions focus on scaling and critical exponents, while less attention is paid to universality, renormalization group flow, and the existence of a unique fixed point, which are the ultimate reasons why scaling theory is so effective in describing continuous phase transitions. We use a combination of Monte Carlo simulations and real space renormalization group theory to determine the renormalization group flow and to show the existence of a universal fixed point in the context of the ferromagnetic Ising model.

I. INTRODUCTION

Continuous phase transitions occur when a material undergoes a spontaneous change in its symmetry or its state. A paradigmatic example of a continuous phase transition is the ferromagnetic transition in which a magnetic material loses its spontaneous magnetization as it is heated beyond the critical temperature. The hallmark of continuous phase transitions is the divergence of the correlation length. How the singular behavior of various thermodynamic quantities, as characterized by critical exponents, is related to the divergence of the correlation length is well described by scaling theory.¹

A particularly intriguing experimental observation is the existence of shared critical properties across different physical systems, characterized by identical critical exponents. For example, different ferromagnetic materials composed of different atoms or possessing distinct crystalline structures exhibit similar behavior close to the critical temperature. The range of applicability of universality is not restricted to ferromagnetic systems and extends to all continuous phase transitions with the same symmetries. Critical opalescence of a liquid close to the critical point is described by the same critical exponents as uniaxial ferromagnets, and the superfluid phase transition shares common features with some ferromagnetic transitions.^{2,3} For this reason continuous phase transitions can be organized into universality classes sharing the same critical exponents.

Close to the transition point the only relevant length scale is the correlation length ξ , and its divergence is solely responsible for the divergencies of various thermodynamic quantities. In this sense, the microscopic details become unimportant in determining the properties of a system close to its critical point, which eventually led to the development of renormalization group theory. In a nutshell, renormalization group theory consists of systematically removing small scale degrees of freedom and observing how their removal affects the large scale physics. This approach can alternatively be interpreted as probing the system at different length scales. The renormalization group flow tracks how the effective theory describing the system changes at different length scales. The aim of this paper is to numerically explore some of these ideas in the context of the Ising model.

The Ising model, which is one of the simplest models exhibiting a ferromagnetic transition, has been extensively used to study the physics of continuous phase transitions. The Ising model is typically taught to test scaling theory and to determine the critical exponents. We

will use the Ising model to study numerically the theoretical foundations of scaling theory and universality in continuous phase transitions, namely the renormalization group. By using a combination of blocking and inverse Ising techniques, we will determine numerically the renormalization group flow and test one of the most intriguing predictions of renormalization group theory: the existence of a fixed point.

We assume that the reader is familiar with the Ising model, with the Markov-chain Monte Carlo technique,⁵ and with some of the basics of renormalization group theory. The paper is organized as follows. In Sec. II we introduce the Ising model, and in Sec. III we review some of the basic ideas of renormalization group theory such as the critical manifold, renormalization group flow, and the fixed point. For a clear and accessible treatment of renormalization group theory the reader may refer to the book by Cardy,² in particular, Chaps. 1 and 3. In Sec. IV we introduce some necessary numerical methods, in particular, a method to efficiently solve the Inverse Ising problem. Finally, in Sec. V we describe a procedure to measure the renormalization group flow and discuss some numerical results.

II. THE ISING MODEL

The Ising model is a minimal model capable of capturing the fundamental aspects of continuous phase transitions. In its original formulation the Ising model describes a system of binary variables, called spins, on a two-dimensional (2D) lattice with nearest-neighbor ferromagnetic interactions. We denote the spins as $\{\sigma_{\mathbf{n}}\}$, where $\mathbf{n} = (n_x, n_y)$, $n_{x,y} = 1, \dots, L$, and L is the linear size of the system. The Boltzmann probability distribution defines the statistical properties of the Ising model,

$$\mathcal{P}[\boldsymbol{\sigma}] = \frac{1}{Z} e^{-\mathcal{H}[\boldsymbol{\sigma}]/k_B T}, \quad \mathcal{H}[\boldsymbol{\sigma}] = -\frac{J}{2} \sum_{|\mathbf{n}-\mathbf{m}|=1} \sigma_{\mathbf{n}} \sigma_{\mathbf{m}}, \quad (1)$$

where the sum $\sum_{|\mathbf{n}-\mathbf{m}|=1}$ is over all pairs of nearest-neighbor spins and the coupling constant $J > 0$. The function \mathcal{H} plays the role of an energy function, and we will improperly call \mathcal{H} the Hamiltonian or the energy.

Depending on the value of the ratio $K = J/k_B T$, the Ising model can be in two distinct phases, which are determined by the magnetization m of the system,

$$m = \frac{1}{L^2} \sum_{\mathbf{n}} \langle \sigma_{\mathbf{n}} \rangle, \quad (2)$$

where the angular brackets indicate the average over the probability distribution in Eq. (1).⁴ The paramagnetic phase ($m \simeq 0$) and the ferromagnetic phase ($m \simeq \pm 1$) are separated by a critical point at which the correlation length ξ diverges. The correlation length is the decay rate of the spatial correlation function,

$$C(\mathbf{n}, \mathbf{m}) = \langle \sigma_{\mathbf{n}} \sigma_{\mathbf{m}} \rangle - \langle \sigma_{\mathbf{n}} \rangle \langle \sigma_{\mathbf{m}} \rangle. \quad (3)$$

Translational symmetry constrains the correlation function to depend only on the distance $|\mathbf{n} - \mathbf{m}| = |n_x - m_x| + |n_y - m_y|$. Therefore,

$$C(r) = \frac{1}{N} \frac{1}{4r} \sum_{|\mathbf{n}-\mathbf{m}|=r} \langle \sigma_{\mathbf{n}} \sigma_{\mathbf{m}} \rangle - \langle \sigma_{\mathbf{n}} \rangle \quad (r > 0), \quad (4)$$

$$C(0) = \frac{1}{N} \sum_{\mathbf{n}} 1 - \langle \sigma_{\mathbf{n}} \rangle^2, \quad (5)$$

where $r = |\mathbf{n} - \mathbf{m}| = |n_x - m_x| + |n_y - m_y|$. The factor of $4r$ accounts for the number of spins at a distance r from a given site at fixed value of \mathbf{n} in two dimensions.

In Fig. 1 we show how the average magnetization m in Eq. (2) depends on the coupling constant K . In Fig. 2 we show how the correlation function $C(r)$ and the correlation length ξ vary with K .

Problem 1: Monte Carlo simulation of the 2D Ising model. Use the Metropolis–Hasting algorithm⁵ and N_s samples $\{\sigma_{\mathbf{n}}(t)\}_{t=1,\dots,N_s}$ from the probability distribution in Eq. (1) with $K = 0.42$ and $L = 128$. Measure the average magnetization m and the correlation function $C(r)$. Fit the latter to an exponential to estimate the correlation length. Repeat the same measurements for different values of K in the range $K \in [0.3, 0.6]$ and determine how m and ξ depend on K . The results should be consistent with the ones shown in Figs. 1 and 2.

III. RENORMALIZATION GROUP THEORY

The conceptual breakthrough that led to a deep theoretical understanding of continuous phase transition was the intuitive idea that in correlated systems with long-range correlations, that is, a divergent correlation length, the details of the microscopic interactions are unimportant when it comes to macroscopic/large-scale properties. If we restrict ourselves to Ising-like models, we can make this statement more concrete by considering the Kadanoff blocking transformation.^{8–10} The Kadanoff blocking transformation involves two

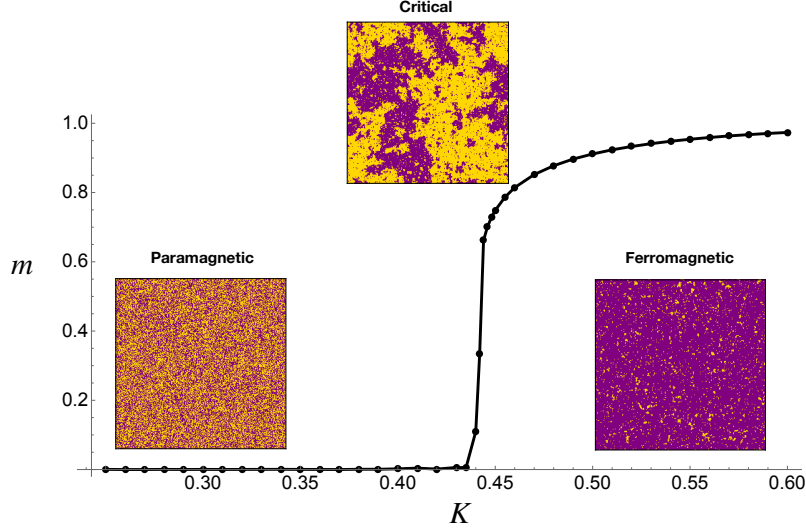


FIG. 1. (Color Online) The magnetization m as a function of the coupling K for the 2D Ising model for $L = 128$ and periodic boundary conditions. The transition between the disordered phase, $m \simeq 0$ for small K , and the ordered phase, $m \simeq 1$ at large K , occurs at $K_c \simeq 0.44$. Also shown is some typical configurations in the disordered and ordered phases and near the critical point. The configurations are obtained using the Metropolis–Hasting algorithm⁶ (see the `IsingRG.py` file in Ref. 7).

steps: coarse graining and rescaling. The first step consists of grouping neighboring spins, within a block of linear dimension b , and defining new block variables $\sigma^{(b)}$ to obtain a coarser description of the system in which small-scale fluctuations are washed away. To be specific, we group spins into $b \times b$ blocks \mathcal{B}_i , each containing b^2 spins, and assign to each of these new block variables a value $\sigma^{(b)} = \pm 1$ according to the majority rule:

$$\sigma_i^{(b)} = \mathcal{M} \left(\sum_{j \in \mathcal{B}_i} \sigma_j \right) \quad (6)$$

$$\mathcal{M}(\sigma) = \begin{cases} +1 & (\sigma > 0) \\ -1 & (\sigma < 0) \\ \text{rnd}(\pm 1) & (\sigma = 0) \end{cases} \quad (7)$$

If the majority of the spins inside the block are $+1$, we set the value of the block variable to 1; if the majority are -1 , we set the value of the block variable to -1 . If b is even and

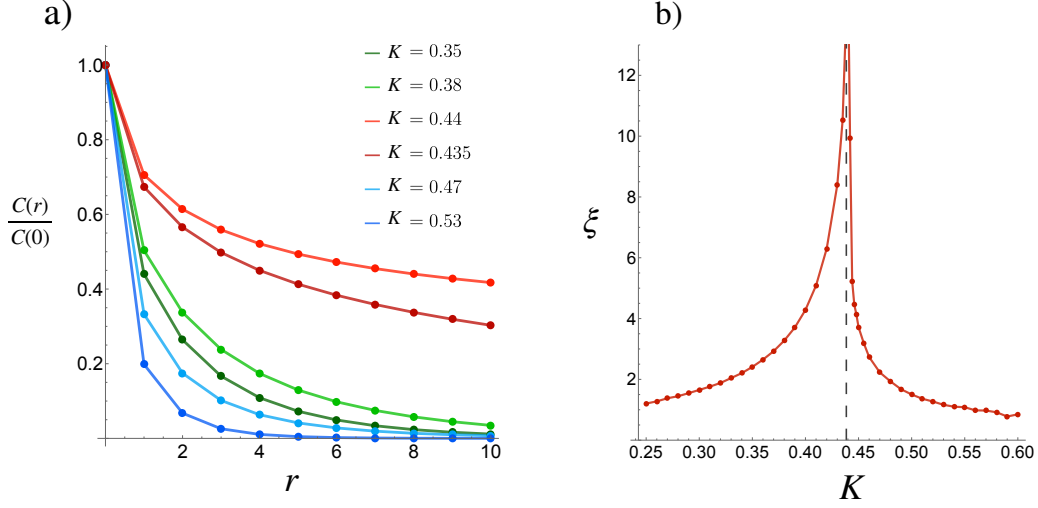


FIG. 2. (a) The correlation function $C(r)$ exhibits a rapid decay in the paramagnetic and ferromagnetic phases, as represented by the green and blue curves respectively. Near the critical point (red curves) the decay of $C(r)$ is notably slower. For convenience, we show the normalized quantity $C(r)/C(0)$. (b) The correlation length is estimated by fitting the exponentially decaying function $e^{-r/\xi}$ to the correlation function. The correlation length ξ diverges at the transition point.

$\sigma = 0$, we randomly choose whether the block variable is ± 1 . We will often refer to this blocking transformation as coarse-graining, and we will refer to the blocked variables as the coarse-grained degrees of freedom. In Fig. 3 we show the affect of the Kadanoff blocking transformation on an equilibrium configuration of the ferromagnetic Ising model for different values of the block size b .

The second step of the Kadanoff blocking transformation is rescaling. The distance between two neighboring spins in the original lattice is exactly one lattice spacing, but after performing a coarse graining with block size b , the distance between two neighboring block variables is now b lattice spacings. Crucially, if we want to compare the original system with the coarse grained one, we have to rescale the coarse grained system by a factor of b . In this way the distance between neighboring block variables remains one lattice spacing for any value of the block size b .

The statistical properties of the coarse-grained configurations are different from those of the original system; measuring the same observable at different levels of coarse graining yields

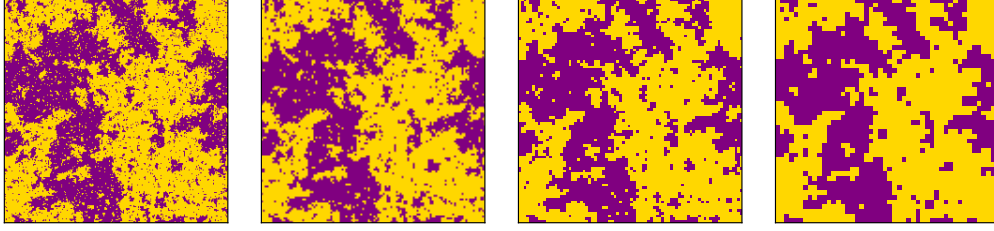


FIG. 3. Effect of the Kadanoff blocking on an equilibrium configuration of the Ising model. The microscopic details are washed away when increasing the block size b . The reader should be able to reproduce these figures by following the “Simulating the Ising model” section of the `MeasureRGflow.ipynb` python notebook in Ref. 7. The effect of the Kadanoff blocking transformation on the Ising model can be better visualized using the program `IsingBlocking.pde` in Ref. 7.

different results.^{2,6} If the original system is described by a Hamiltonian $\mathcal{H}[\sigma]$, the effective Hamiltonian $\mathcal{H}_b[\sigma^b]$ describing the coarse-grained degrees of freedom is in general different at each level of coarse-graining. How the Hamiltonian changes under coarse-graining is called the renormalization group flow.

A. Critical manifold, renormalization group fixed point, and universality

The renormalization group flow, which is how the Hamiltonian changes at different levels of coarse-graining, is the key to understanding universality and the effectiveness of the scaling theory. The qualitative behavior of the renormalization group flow depends on how close the system is to the critical point. We can distinguish three qualitatively different scenarios depending on whether the system is in the paramagnetic or ferromagnetic phase or at the critical point.

In the paramagnetic phase the magnetization is zero and the spins are weakly correlated. As the coarse-graining process progresses, the system will converge toward block variables that are random and uncorrelated. Therefore, the Hamiltonian of the system flows toward a completely random model, which can be interpreted as either at an infinite temperature or a zero coupling fixed point. In the ferromagnetic phase, coarse-graining leads to block variables that are more and more ordered, and thus the Hamiltonian flows to a strongly coupled model, which may be interpreted as a zero temperature fixed point. Both these

scenarios are trivial (zero or infinity) and not very exciting. The renormalization group flow becomes more interesting close to the critical point, which divides the paramagnetic and the ferromagnetic phases. In this case the renormalization group flow will approach neither of the trivial fixed points, but will converge to the nontrivial finite fixed point.

We now consider an example of an Ising model with nearest-neighbor K_1 and next-nearest neighbor K_2 interactions. If both K_1 and K_2 are very small, the system is in the paramagnetic phase. Conversely, if the couplings are sufficiently large, the system is in the ferromagnetic phase. We can think of doing three numerical experiments, which are summarized in Fig. 4. The first experiment consists of choosing $K_2 = 0$ and gradually increasing K_1 (green curve); eventually K_1 will be large enough to cross a critical point of the type

$$K_1 = K_1^c \quad K_2 = 0, \quad (8)$$

and enter the ferromagnetic phase. For the second numerical experiment we keep $K_1 = 0$ and gradually increase K_2 (blue curve). As in the previous case, we will eventually enter the ferromagnetic phase after crossing a critical point of the type,

$$K_1 = 0 \quad K_2 = K_2^c. \quad (9)$$

Finally, we can start with small K_1 and K_2 and increase both of them gradually. In this case we also expect to cross a critical point with both K_1 and K_2 different from zero.

Note that there is no unique critical point, in the sense that the values of the couplings corresponding to a system with infinite correlation length are not unique. We can convince ourselves that there are infinitely many possible combinations of the parameters K_1, K_2 for which the system is at the critical point. We call the *critical manifold* the set of values of the couplings K_1, K_2 for which the correlation length $\xi(K_1, K_2)$ is infinite. The prediction of renormalization group theory is that the renormalization group flow converges to the same universal fixed point independently of the specific values of K_1 and K_2 if they are on the critical manifold $\xi(K_1, K_2) = \infty$.

This behavior can be summarized in the renormalization group flow diagram shown in Fig. 5, which describes how the parameters of the model change under a coarse-graining transformation. The general picture we obtain from Fig. 5 is that in the ferromagnetic and paramagnetic phases the renormalization group flow converges to trivial fixed points, which are the strong coupling $\mathbf{K} = \infty$ and zero coupling regime $\mathbf{K} = 0$, respectively. Con-

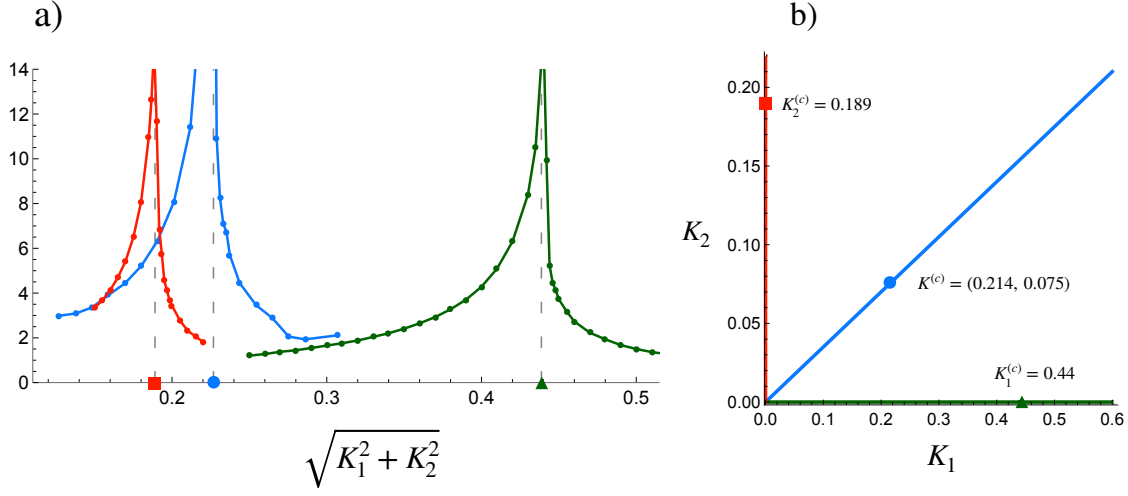


FIG. 4. (Color online) The correlation length for a $L = 128$ Ising model with periodic boundary conditions. We scan the parameter space in three directions and measure the correlation length ξ . (a) The red, green, and blue curves correspond to scanning the (K_1, K_2) plane on the K_2 axis, K_1 axis, and on the $K_2 = 0.35 \times K_1$ line as shown in (b), respectively. All three cases cross a critical point with a divergent correlation length.

versely, on the critical manifold (red curve) where the correlation length ξ diverges, the renormalization group flow converges to a unique fixed point (red dot), which is independent of the specific value of the model's parameters before applying the coarse-graining transformation.¹⁵ For this reason different systems display the same behavior close to a critical phase transition, because their large scale physics is described by the same fixed point theory.

We can think of this Kadanoff blocking procedure as a thought experiment or a theoretical tool to study critical phase transitions. If we take this picture seriously, we should be able to actually measure the renormalization group flow. Although the scaling theory predicted by renormalization group theory can be easily tested numerically, it is not immediately obvious how to measure the renormalization group flow and show that all systems on the critical manifold converge to the same fixed point.

To measure how various observables scale under coarse-graining is straightforward. We

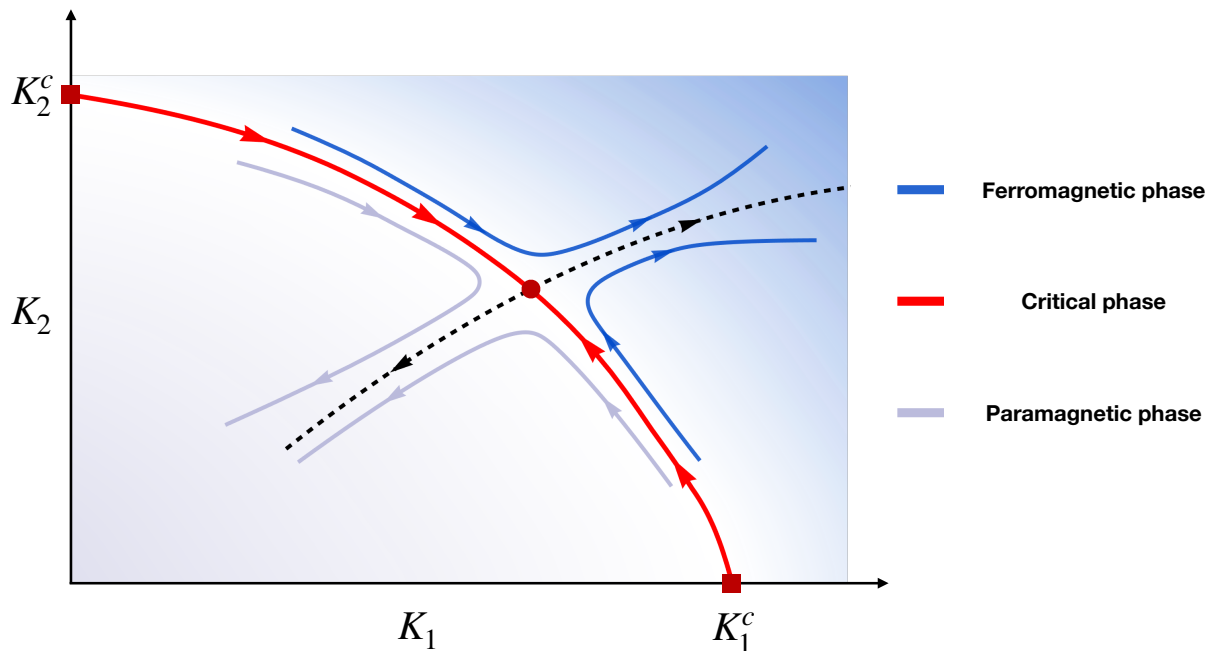


FIG. 5. (Color online) Qualitative sketch of the renormalization group flow of a 2D Ising model with nearest-neighbor K_1 and next-nearest-neighbor K_2 interactions. The arrows show how the model's parameters evolve under coarse-graining. The qualitative behavior of the renormalization group flow depends on the value of the parameters (K_1, K_2) . When the couplings are large (blue region), the system is in a ferromagnetic state and the renormalization group flow (blue curves) flows to a strongly interacting model $\mathbf{K} \rightarrow \infty$. When the couplings are small, (gray region) the system is in the paramagnetic phase, and the renormalization group flow (gray curves) drives the system to a non-interacting $\mathbf{K} = 0$ model. In the critical regime, or more precisely, on the critical manifold $\xi(K_1, K_2) = \infty$, the renormalization group flow converges to a universal fixed point (red dot) which is independent of the particular value of the pair (K_1, K_2) . For example, the two systems with coupling $(K_1^c, 0)$ and $(0, K_2^c)$ both converge to the same fixed point.

just have to measure the same observables at different levels of coarse-graining.⁶ It is less clear how to measure how the model's parameters, or the effective Hamiltonian, change under coarse-graining.

To tackle this problem in a slightly different context, Shenker and Tobochnik¹¹ used an ingenious strategy using a Monte Carlo renormalization group approach which involves comparing the effect of the blocking transformation on systems of different sizes and parameters.

In this way they estimated the beta-functions of the model. The beta functions describe how the effective description of the system changes with the length scale at which we probe the system, and are intimately connected to the renormalization group flow.¹² Remarkably, this approach made possible extracting information on the structure of the renormalization group flow in a time with very limited computational resources. We will use a different approach, which involves solving the inverse Ising problem.

Problem 2. Magnetization distribution and blocking transformation. (a) From the Ising model configurations of Problem 1 determine the histogram of the magnetization m for various values of the coupling K . Discuss how the histogram of the magnetization differs in the paramagnetic and ferromagnetic phases and near the critical point. (b) Apply the Kadanoff blocking transformation to the same configurations with $b = 2$, and determine the histogram of the distribution of the magnetization of the blocked system, $m = \sum_{\mathbf{n}} \sigma_{\mathbf{n}}^{(b)}$. Repeat this procedure for $b = 2, 3, 4, 5$, and discuss how the effect of the Kadanoff blocking transformation differs in the three regions. Is this behavior consistent with the theoretical prediction of Fig. 5?

Problem 3: Ising model with next-nearest neighbor interactions. Simulate a $L = 120$ Ising model with $K_1 = 0.16$ and $K_2 = 0.04$

$$\mathcal{P}(\boldsymbol{\sigma}) = \frac{1}{Z} \exp \left(\frac{1}{2} K_1 \sum_{|\mathbf{n}-\mathbf{m}|=1} \sigma_{\mathbf{n}} \sigma_{\mathbf{m}} + \frac{1}{2} K_2 \sum_{|\mathbf{n}-\mathbf{m}|=2} \sigma_{\mathbf{n}} \sigma_{\mathbf{m}} \right), \quad (10)$$

and measure the magnetization and the correlation length. Increase K_1 and K_2 on the line $K_1/K_2 = 4$ and determine how m and ξ change.

IV. THE INVERSE ISING PROBLEM

Given a spin Hamiltonian $\mathcal{H}[\boldsymbol{\sigma}]$ and $\beta \equiv 1/k_B T$, we can sample equilibrium configurations of the probability distribution $\mathcal{P} = e^{-\beta \mathcal{H}[\boldsymbol{\sigma}]} / Z$ using a Markov-chain Monte Carlo algorithm,⁶ and compute its moments and correlations such as,

$$\mu_{\mathbf{n}} = \langle \sigma_{\mathbf{n}} \rangle \quad C_{\mathbf{n}\mathbf{m}} = \langle \sigma_{\mathbf{n}} \sigma_{\mathbf{m}} \rangle. \quad (11)$$

Sampling from the probability distribution is what we call the direct Ising problem. In the inverse Ising problem the quantities in Eq. (11) or some equilibrium samples of an Ising

model $\{\sigma_{\mathbf{n}}(t)\}$ are given and one computes the Hamiltonian \mathcal{H} that would generate these moments and correlations. In particular, given N_s independent samples of the form,

$$\{\sigma_{\mathbf{n}}(t)\}_{n=1,\dots,L^2}^{t=1,\dots,N_s}, \quad (12)$$

where \mathbf{n} labels the position on the lattice and t labels the samples, we wish to find the probability distribution $\mathcal{P}^* \propto e^{-\mathcal{H}^*}$, or better the Hamiltonian \mathcal{H}^* , that most likely generated the data. Here we have incorporated β into \mathcal{H}^* .

A. Maximum likelihood

One way of finding the Hamiltonian \mathcal{H}^* that best fits the data is to use the maximum likelihood approach. This approach consists of finding the probability distribution \mathcal{P}_{ML} that most likely generated the data. One difficulty is that the space of possible probability distributions of L^2 binary variables is quite large ($2^{L^2} - 1$ degrees of freedom, corresponding to every possible state of the system). A possible way out is to make some assumptions for the form of \mathcal{H} . For instance, we are interested only in systems with translational invariance and \mathbb{Z}_2 symmetry. These requirements imply that the only terms allowed in \mathcal{H} must contain an even number of spins and their interaction depends only on the distance between spins. An example of such an Hamiltonian is

$$-\mathcal{H}[\sigma] = \frac{1}{2} \sum_{\mathbf{n}, \mathbf{m}} K_{|\mathbf{n}-\mathbf{m}|} \sigma_{\mathbf{n}} \sigma_{\mathbf{m}}, \quad (13)$$

where K_d is the coupling constant between spins separated by a distance d . The form in Eq. (13) is just an ansatz because there are many other terms that could have been included, but for simplicity, we will consider only Hamiltonians of the form in Eq. (13).

We will simplify the problem even further. In a system of linear dimension L the maximum distance between two spins is $d = L$, and, in principle, we should take into account L possible couplings $\{K_1, \dots, K_L\}$. We will assume that the couplings are zero greater than a certain distance d_{max} . In all the numerical results shown in the following we use $d_{\text{max}} = 4$.

Finding the Hamiltonian of the form in Eq. (13) that is most likely to generate the data in Eq. (12) is a well posed question. Given the couplings $\mathbf{K} = \{K_1, K_2, \dots, K_{d_{\text{max}}}\}$, the

probability of observing a given configuration σ is,

$$\mathbb{P}(\sigma|\mathbf{K}) = \frac{1}{Z(\mathbf{K})} \exp \left(\frac{1}{2} \sum_{n,m} K_{|n-m|} \sigma_n \sigma_m \right) \quad , \quad (14)$$

$$Z(\mathbf{K}) = \sum_{\sigma} \exp \left(\frac{1}{2} \sum_{n,m} K_{|n-m|} \sigma_n \sigma_m \right). \quad (15)$$

Therefore, the probability of observing the data in Eq. (12) is,

$$\mathbb{P}(\text{data}|\mathbf{K}) = \prod_{t=1}^{N_s} \frac{1}{Z} \exp \left(\frac{1}{2} \sum_{n,m} K_{|n-m|} \sigma_n(t) \sigma_m(t) \right). \quad (16)$$

We use Bayes' theorem, or simply the property of conditional probabilities $p(x|y)p(y) = p(y|x)p(x)$, and obtain

$$\mathbb{P}(\mathbf{K}|\text{data}) = \frac{\mathbb{P}(\text{data}|\mathbf{K})\mathbb{P}(\mathbf{K})}{\mathbb{P}(\text{data})}, \quad (17)$$

where $\mathbb{P}(\text{data})$ is the probability of the data averaged over all possible parameters \mathbf{K} ; $\mathbb{P}(\mathbf{K})$ is the a priori probability of the parameters \mathbf{K} , and for this reason is called *prior*. The quantity in Eq. (17) is the *likelihood* and represents the probability that the data in Eq. (12) have been generated by a model of the type in Eq. (13) with parameters \mathbf{K} .

The maximum likelihood approach consists of finding the value of the couplings \mathbf{K}^* that maximizes the likelihood,

$$\mathbf{K}^* = \max_{\mathbf{K}} \mathbb{P}(\mathbf{K}|\sigma). \quad (18)$$

If we assume that the prior $\mathbb{P}(\mathbf{K})$ is constant, and because the probability of the data $\mathbb{P}(\text{data})$ is independent of \mathbf{K} , the likelihood in Eq. (17) takes the form,

$$\mathbb{P}(\mathbf{K}|\text{data}) = \mathbb{P}_0 \prod_{t=1}^{N_s} \frac{1}{Z} \exp \left(\frac{1}{2} \sum_{n,m} K_{|n-m|} \sigma_n(t) \sigma_m(t) \right), \quad (19)$$

where \mathbb{P}_0 is a constant independent of \mathbf{K} . It is useful to define the logarithm of the likelihood $\mathcal{L}(\mathbf{K}) = \frac{1}{N_s} \ln(\mathbf{K}|\text{data})$, which up to a constant term is

$$\mathcal{L}(\mathbf{K}) = \frac{1}{2} \frac{1}{N_s} \sum_{t=1}^{N_s} \sum_{n,m} K_{|n-m|} \sigma_n(t) \sigma_m(t) - \ln(Z). \quad (20)$$

The solution of the inverse Ising problem is given by the value of \mathbf{K} that maximizes $\mathcal{L}(\mathbf{K})$.

B. The solution of the maximum likelihood problem

The solution \mathbf{K}^* of the maximum likelihood problem is the stationary points of the likelihood and satisfies

$$\frac{\partial \mathcal{L}(\mathbf{K})}{\partial K_d} = 0 \quad (d = 1, \dots, d_{\max}), \quad (21)$$

where the derivative of the log-likelihood is given by

$$\frac{\partial \mathcal{L}(\mathbf{K})}{\partial K_d} = 2d [C_{\text{data}}(d) - C_{\mathbb{P}}(d; \mathbf{K})]. \quad (22)$$

$C_{\mathbb{P}}(d; \mathbf{K})$ is the correlation function at distance d computed using the probability distribution in Eq. (14) and $C_{\text{data}}(d)$ is the correlation function computed from the data,

$$C_{\mathbb{P}}(d; \mathbf{K}) = \frac{1}{Z} \sum_{\boldsymbol{\sigma}} \frac{1}{4d} \sum_{|\mathbf{n}-\mathbf{m}|=d} \sigma_{\mathbf{n}} \sigma_{\mathbf{m}} e^{\frac{1}{2} \sum_{\mathbf{n}, \mathbf{m}} K_{|\mathbf{n}-\mathbf{m}|} \sigma_{\mathbf{n}} \sigma_{\mathbf{m}}} \quad (23)$$

$$C_{\text{data}}(d) = \frac{1}{N_s} \sum_{t=1}^{N_s} \frac{1}{4d} \sum_{|\mathbf{n}-\mathbf{m}|=d} \sigma_{\mathbf{n}}(t) \sigma_{\mathbf{m}}(t). \quad (24)$$

The maximum of the likelihood can be found iteratively using the gradient descent technique, which is a standard method of numerically finding the maximum/minimum of a function. We start from a random value of the couplings \mathbf{K} and iteratively update the couplings according to the rule,

$$\mathbf{K}' = \mathbf{K} + \eta \frac{\partial \mathcal{L}(\mathbf{K})}{\partial \mathbf{K}}. \quad (25)$$

The gradient descent technique might fail if the function we are maximizing has many local maxima. In this case, the solution we find depends on the random initialization, and there is no guarantee that we will find the global maximum of the function. In our case, it can be shown that the likelihood \mathcal{L} is a strictly concave function with a unique maximum.¹³ Therefore, if we iterate Eq. (25), the couplings \mathbf{K} converge to the maximum likelihood solution Eq. (21).¹³ The parameter η is called the learning rate, and determines how fast we approach the solution $\partial_{\mathbf{K}} \mathcal{L} = 0$. Ideally, we would like to choose η as high as possible, but if η is too large, the gradient descent algorithm might become unstable.

We still have a problem finding the maximum because we have to iterate Eq. (25) many times for \mathbf{K} to converge, and at each iteration we have to compute $C_{\mathbb{P}}$, meaning that we have to sample from the probability distribution Eq. (14). Computing moments of Eq. (14)

requires using Monte Carlo methods. It is evident that this approach is computationally costly.

Problem 4: The maximum likelihood equation. Derive Eq. (22) by explicitly taking the derivative of the log-likelihood Eq. (20) with respect to K_d .

C. Maximum pseudo-likelihood

The algorithm we now describe is an adaptation of Auerll and Ekeberg.¹⁴ Again we compute the set $\boldsymbol{\sigma}$ of N_s independent samples of a 2D Ising model of linear dimension L . Our goal is to find a model of the form Eq. (13) that describes the experimental data in Eq. (12). For each of the variables $\sigma_{\mathbf{n}}$ we consider the conditional probability of $\sigma_{\mathbf{n}}$ given all the other variables. This probability is given by,

$$\mathcal{P}(\sigma_{\mathbf{n}}|\boldsymbol{\sigma}_{\setminus\mathbf{n}};\mathbf{K}) = \frac{1}{1 + e^{-2\sigma_{\mathbf{n}}H_{\mathbf{n}}}} \quad H_{\mathbf{n}} = \sum_{\mathbf{m}} K_{|\mathbf{n}-\mathbf{m}|}\sigma_{\mathbf{m}}, \quad (26)$$

where $H_{\mathbf{n}}$ is the local field acting on spin $\sigma_{\mathbf{n}}$, and $\boldsymbol{\sigma}_{\setminus\mathbf{n}}$ is the set of all spins except the spin at site \mathbf{n} . If we consider $\sigma_{\mathbf{n}}$ as the dependent variable, and the complementary set $\boldsymbol{\sigma}_{\setminus\mathbf{n}}$ is taken as independent variables, the maximum likelihood estimator for \mathbf{K} is

$$\ell_{\mathbf{n}}(\mathbf{K}) = \frac{1}{N_s} \sum_{t=1}^{N_s} \ln \mathcal{P}(\sigma_{\mathbf{n}}^t|\boldsymbol{\sigma}_{\setminus\mathbf{n}}^t;\mathbf{K}), \quad (27)$$

where $\sigma_{\mathbf{n}}^t = \sigma_{\mathbf{n}}(t)$. We define the pseudo-likelihood $\mathcal{L}_P(\mathbf{K})$ of the system as

$$\mathcal{L}_P(\mathbf{K}) = \sum_{\mathbf{n}} \ell_{\mathbf{n}}(\mathbf{K}). \quad (28)$$

Similar to what we described for the maximum likelihood approach, the solution of the inverse Ising problem is given by the maximum of the pseudo-likelihood,

$$\mathbf{K}^{\star} = \operatorname{argmax}_{\mathbf{K}} \mathcal{L}_P(\mathbf{K}) \quad (29)$$

$$\frac{\partial \mathcal{L}_P(\mathbf{K}, \boldsymbol{\sigma})}{\partial K_d} = \frac{2}{L^2 N_s} \sum_{t=1}^{N_s} \sum_{\mathbf{n}} \sum_{|\mathbf{n}-\mathbf{m}|=d} \frac{\sigma_{\mathbf{n}}(t)\sigma_{\mathbf{m}}(t)}{1 + e^{-2\sigma_{\mathbf{n}}(t) \sum_{\mathbf{l}} K_{|\mathbf{l}-\mathbf{n}|}\sigma_{\mathbf{l}}(t)}}. \quad (30)$$

As we did to find the solution of the maximum likelihood problem, we can find the solution to the pseudo-likelihood problem using a gradient descent algorithm. Hence, we iterate the equation,

$$K'_d = K_d + \eta \frac{\partial \mathcal{L}_P(\mathbf{K}, \boldsymbol{\sigma})}{\partial K_d} \quad (d = 1, \dots, d_{\max}). \quad (31)$$

However, in this case we can compute the gradient of the likelihood directly from the data using Eq. (30).

Equation (31) implements the simplest possible optimization scheme and is sufficient to solve our simple problem. For more complex problems more sophisticated techniques are usually needed.¹³ Surprisingly, even if the log pseudo likelihood (28) is just an approximation of the log likelihood (20), it can be proven that in the large sample size limit (see Problem 5) the pseudo-likelihood maximization method gives the correct solution.

We can check that the pseudo-likelihood inference scheme works as expected. We generate independent equilibrium configurations from an Ising model with just nearest-neighbor K_1 and next-nearest neighbor K_2 interactions, and check whether or not the pseudo-likelihood inference method can correctly retrieve the couplings from the configurations. The results are shown in Fig. 6.

Problem 5: Correctness of the pseudo-likelihood approach. Assume that you have a very large sample, $\{\sigma_{\mathbf{n}}(t)\}_{\mathbf{n}=1,\dots,L^2}^{t=1,\dots,N_s}$, $N_s \rightarrow \infty$, extracted from a probability distribution of the form Eq. (14) and with couplings $\tilde{\mathbf{K}}$. Show that $\mathcal{L}_P(\mathbf{K})$ in Eq. (28) is a maximum at $\mathbf{K} = \tilde{\mathbf{K}}$ (Hint: show that in this case the derivative of the pseudo-likelihood in Eq. (30) is zero at $\mathbf{K} = \tilde{\mathbf{K}}$).

Problem 6: Testing the pseudo-likelihood approach. Apply the pseudo-likelihood maximization approach, with $\eta = 0.02$, to the data generated in Problems 1 and 3 to retrieve the coupling constants used in running the simulations.

V. MEASURING THE RENORMALIZATION GROUP FLOW

Our goal is to measure numerically the renormalization group flow, given that we have all the necessary tools. The strategy we will use is straightforward. We sample independent equilibrium configurations, Eq. (10), from a 2D Ising model with nearest neighbor K_1 and next-nearest neighbor K_2 interactions with periodic boundary conditions. Then we coarse grain the configurations of the system according to the Kadanoff blocking rule in Eq. (7); that is, we group variables in blocks of size b and obtain the blocked configurations $\sigma^{(b)}(t)$

$$\sigma^{(b)} = \{\sigma_i(t)\}_{i=1,\dots,(L/b)^2}^{t=1,\dots,N_s}. \quad (32)$$

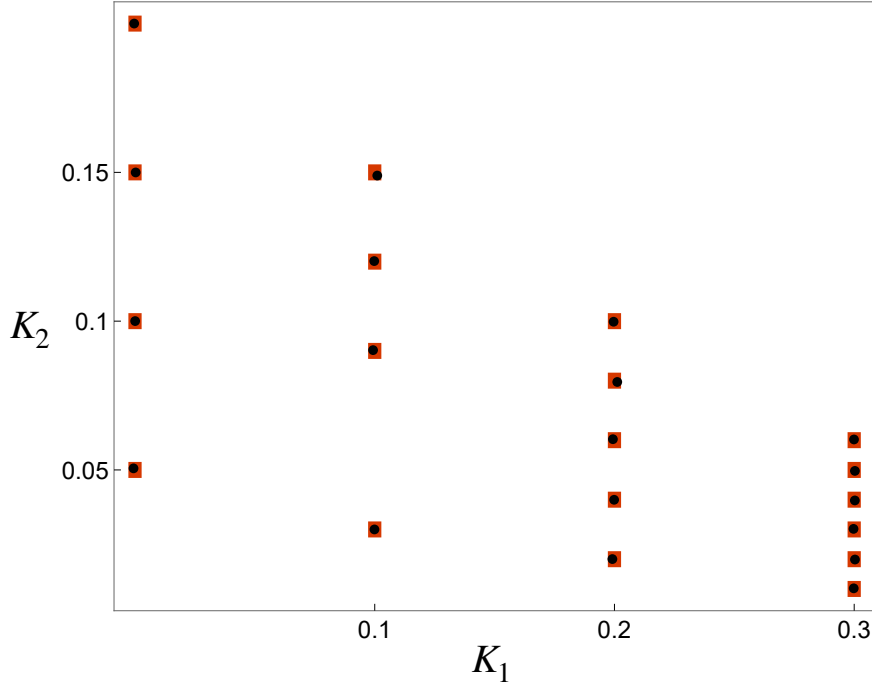


FIG. 6. Testing the pseudo-likelihood maximization inference method. The red squares are the values of the couplings (K_1, K_2) used to generate the samples, the black dots correspond to the parameters retrieved by the configurations, obtained by maximizing the pseudo-likelihood \mathcal{L}_P in Eq. (28) using $d_{\max} = 4$. The data are from a simulation of the 2D Ising model with $L = 120$ and periodic boundary conditions. The reader should be able to reproduce these results using the “Inference-Inverse Ising Problem” section of the MeasureRGflow.ipynb python notebook in Ref. 7.

Note that in a finite-size system the coarse-graining procedure reduces the linear size of the system by a factor of b .

At this point, we can apply the inverse Ising method described in Sec. IV to infer the parameters that would have generated the coarse-grained data in Eq. (32). The result of the inference is the effective theory at the b th level of coarse-graining. We repeat this procedure for increasing values of the coarse-graining block size. In this way, we measure how the parameters of the model change under coarse-graining; that is, we are measuring the renormalization group flow. This procedure is summarized in Fig. 7.

We usually think of the renormalization group as an iterative procedure. We iterate the Kadanoff blocking transformation, and after each iteration, we obtain a coarser description

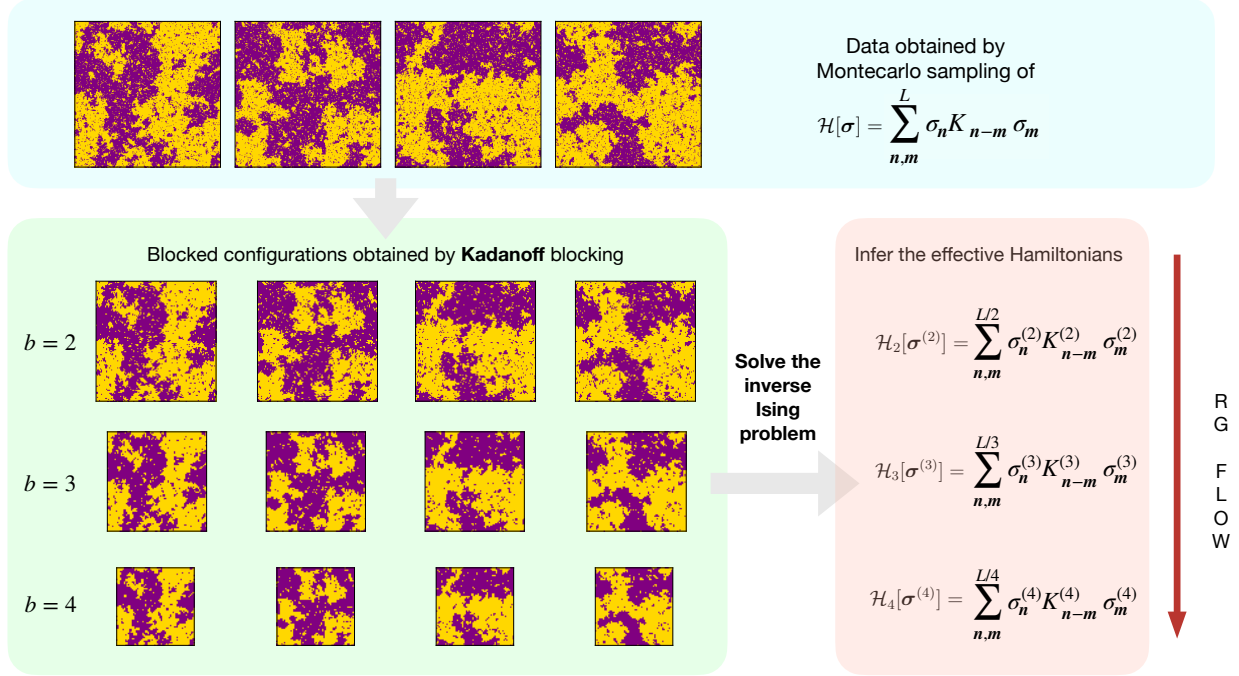


FIG. 7. Summary of the numerical method used to measure the renormalization group flow. We sample equilibrium configurations from an equilibrium Ising model (blue) and apply the Kadanoff blocking rule in Eq. (7) for increasing values of the block size b to obtain a coarser and coarser description of the system in which small scale fluctuations are integrated out (green). Finally, we apply the inverse Ising procedure to infer the Hamiltonian that would have generated the coarse grained data (red). The result of this procedure is the renormalization group flow of the system, which is how the effective theory changes at different levels of coarse-graining.

of the system. If the linear dimension of the system is L , and we iterate the blocking transformation with $b = 2$, we obtain coarse grained systems of sizes $L/2$, $L/4$, $L/8$, and so on. If we compare the coarse grained systems to the original one, this procedure corresponds to block sizes $b = 2, 4, 8, \dots$. The main downside of this approach is that the size of the system decreases exponentially with the number of renormalization group steps (the number of Kadanoff blocking iterations). An alternative is to apply the blocking transformation to the original system for increasing values of the block size $b = 2, 3, 4, 5, 6, \dots$. In this way we obtain blocked systems of sizes $L/2$, $L/3$, $L/4, \dots$. By using this strategy the size of the system decreases linearly with the number of steps, and for this reason we adopt the latter strategy.

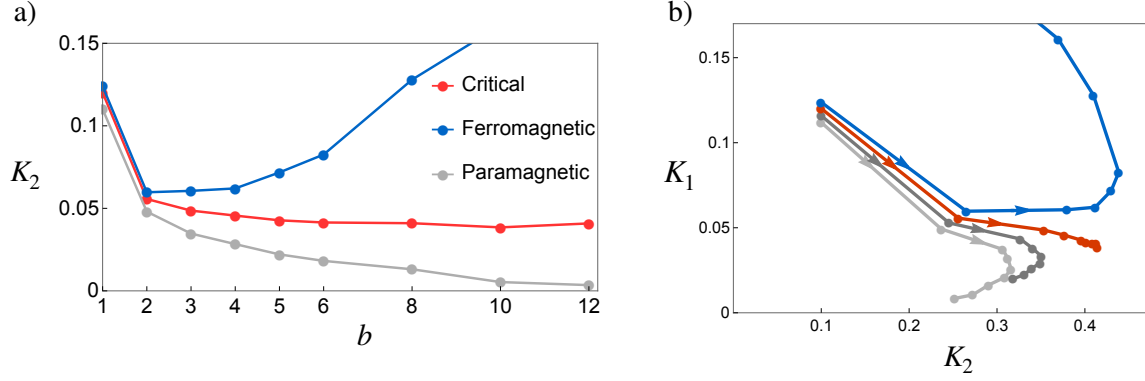


FIG. 8. Numerical renormalization group flow. (a) Flow of the next-nearest neighbor coupling K_2 as a function of the block size b , with $K_1 = 0.1$ for different initial values of K_2 . Depending on the value of K_2 , we observe different qualitative behavior of $K_2^{(b)}$ for large b : $K_2^{(b)} \rightarrow 0$ paramagnetic phase (gray curve), $K_2^{(b)} \rightarrow \infty$ ferromagnetic phase (blue curve), and $K_2^{(b)} \rightarrow K_2^*$ critical regime (red curve). (b) Renormalization group flow projected on the (K_1, K_2) plane; the arrow goes toward increasing values of b . Different colors correspond to different regions of parameter space: paramagnetic (gray), ferromagnetic (blue), and critical (red). The numerical renormalization group flow is compatible with the qualitative picture of Fig. 5. Data are for an initial value of $L = 480$ and $N_s = 3 \times 10^3$. The reader should be able to reproduce these results following the MeasureRGflow.ipynb python notebook in Ref. 7.

We first simulate a system of size $L = 480$ for different values of the couplings (K_1, K_2) . In particular, we fix $K_1 = 0.1$ and simulate systems with different values of K_2 . For each of these simulations, we perform the blocking transformation with block sizes $b = 2, 3, 4, 5, 8, 10, 12$ and, following the procedure described in Fig. 7, we measure the resulting renormalization group flow. The results are summarized in Fig. 8. We first note that the simulations reproduce correctly the qualitative picture illustrated in Fig. 5. We can clearly distinguish the different qualitative behavior depending on the phase of the system. In the paramagnetic phase (gray curves) the flow converges to infinite temperature or zero coupling theory. In the ferromagnetic phase (blue curve) the flow converges to a zero temperature (strong coupling) theory. Finally, as predicted by the theory, in the critical regime (red curve) the flow converges to a finite fixed point. This behavior implies that in the critical regime the renormalization group flow converges to a finite fixed point.

We still need to show that this fixed point is unique and that any renormalization group flow trajectory starting on the critical manifold converges to the same fixed point. Different pairs (K_1, K_2) can correspond to a critical Ising model, with a divergent correlation length ξ , as shown in Fig. 4. In this numerical experiment we simulate the Ising model with three pairs of couplings (K_1, K_2) , carefully tuned to be on the critical manifold. The prediction of renormalization group theory is that the flow converges to the same fixed point. As before, we apply the blocking transformation with block sizes $b = 2, 3, 4, 5, 8, 10, 12$ and determine the resulting renormalization group flow. The results are shown in Fig. 9. In agreement with the theoretical picture in Eq. (5), the three trajectories converge to the same fixed point. The yellow curve starts from $(K_1 = 0.44, K_2 = 0)$, meaning that at the beginning of the renormalization group flow the system does not have any next-nearest neighbor interactions, $K_2 = 0$. The next-nearest neighbor interaction is generated by the coarse graining procedure, which is an example of an interaction term that is generated by the renormalization group. Also, interactions at larger distances are generated such as K_3 and K_4 . In the numerical experiment showed in Fig. 9 the fixed point is at $K_3 = 0.011$ and $K_4 = 0.031$. Interestingly the fixed point values of the higher distance couplings are significantly different from zero. The dominant term in the expansion is the nearest neighbors coupling K_1 , which is an order of magnitude larger.

The numerical experiment we have presented is restricted to the Ising model. However, renormalization group theory predicts that a similar mechanism explains universality in more realistic systems, and that the very same fixed point theory shown in Fig. 9 also describes the critical properties of some real ferromagnets.²

VI. CONCLUSION

By using a combination of Markov-chain Monte Carlo, Kadanoff blocking, and inverse Ising model calculations, we were able to study the renormalization group flow in the ferromagnetic Ising model. The results are in agreement with renormalization group theory.² The numerical experiments could be helpful for consolidating the reader's understanding of renormalization group theory. Although renormalization group theory has been tested in several contexts, to the best of my knowledge, this is the first time that this particular aspect of the renormalization group has been studied numerically, which may be attributed

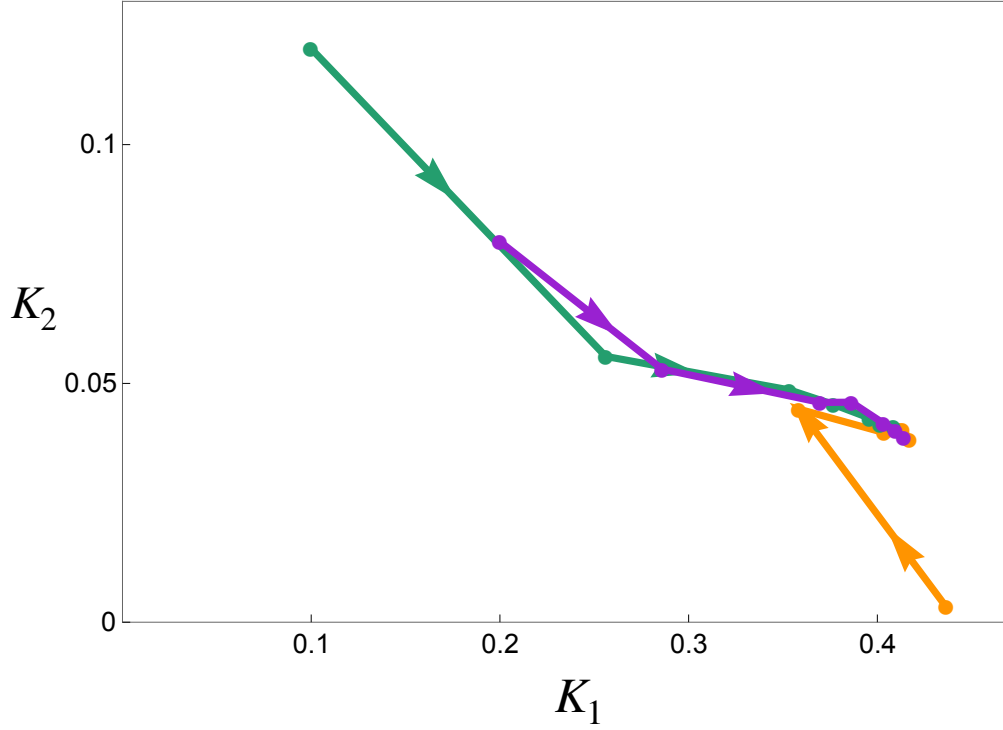


FIG. 9. The renormalization group on the critical manifold. Three trajectories, relative to (K_1, K_2) on the critical manifold. Any renormalization group flow trajectory that starts on the critical manifold converges to the same fixed point, independently of the initial value of the pair (K_1, K_2) . Data for $L = 480$ and $N_s = 3 \times 10^3$.

to the fact that, during the early stages of the development of renormalization group theory, the inverse Ising model techniques were not yet developed and the computational power was insufficient for such a numerical experiment. It is fascinating how the numerical results match perfectly with the theoretical predictions that were conceived almost fifty years ago.

ACKNOWLEDGMENTS

I thank F. Ferretti, R. Pang and F. G. Castro for comments upon reading the manuscript. I thank A. Cavagna for fruitful discussions and U. Tauber for suggesting the publication of

this manuscript.

-
- ¹ Benjamin Widom, “Equation of state in the neighborhood of the critical point,” J. Chem. Phys. **43**, 3898–3905 (1965).
- ² John Cardy, *Scaling and Renormalization in Statistical Physics* (Cambridge University Press, 1996).
- ³ Mehran Kardar, *Statistical Physics of Fields* (Cambridge University Press, 2007).
- ⁴ Computing averages over the Ising probability distribution in Eq. (1) is not trivial. The reason is that the number of possible configurations $C = 2^{L^2}$ of the system is exponentially large with the number of spins. It is possible to numerically sample the probability distribution using the Markov-chain Monte Carlo technique.^{5,6}
- ⁵ David Landau and Kurt Binder, *A Guide to Monte Carlo Simulations in Statistical Physics* (Cambridge University Press, 2021).
- ⁶ Mark E. J. Newman and Gerard T. Barkema, *Monte Carlo Methods in Statistical Physics* (Clarendon Press, 1999).
- ⁷ The supplemental material can be downloaded from the github repository <<https://github.com/lucadic/IsingCG.git>>. The supplemental material contains the python file IsingRG.py with functions to simulate a 2D Ising model using the Metropolis–Hasting algorithm to solve the inverse Ising problem and to apply the blocking coarse graining transformation. In the python notebook MeasureRGFlow.ipynb are the functions we used to reproduce most of the plots shown in the main text. In addition, we provided a Javascript (and Java) application to visualize the effect of the Kadanoff blocking transformation (see the readme.txt file), which can be downloaded from the github repository or accessed at <<https://lucadic.github.io/IsingCG/>>.
- ⁸ Leo P. Kadanoff, “Scaling laws for Ising models near T_c ,” Physics Physique Fizika **2**, 263–272 (1966).
- ⁹ Leo P. Kadanoff et al., “Static phenomena near critical points: Theory and experiment,” Rev. Mod. Phys. **39**, 395–431 (1967).
- ¹⁰ Kenneth G. Wilson, “The renormalization group and critical phenomena,” Rev. Mod. Phys. **55**, 583–600 (1983).

- ¹¹ Stephen H. Shenker and Jan Tobochnik, “Monte Carlo renormalization-group analysis of the classical Heisenberg model in two dimensions,” *Phys. Rev. B* **22**, 4462–4472 (1980).
- ¹² Nigel Goldenfeld, *Lectures on Phase Transitions and the Renormalization Group* (CRC Press, 2018).
- ¹³ H. Chau Nguyen, Riccardo Zecchina, and Johannes Berg, “Inverse statistical problems: from the inverse Ising problem to data science,” *Adv. Phys.* **66**, 197–261 (2017).
- ¹⁴ Erik Aurell and Magnus Ekeberg, “Inverse Ising inference using all the data,” *Phys. Rev. Lett.* **108**, 090201 (2012).
- ¹⁵ How trajectories that are close to the critical regime run away from the critical manifold determines the scaling properties of the system. We will not focus on this particular aspect; more details can be found in standard textbooks such as Chaps. 3 of Ref. 2 and Chap. 4 of Ref. 3.